# Reconstructing Quantum States With Quantum Reservoir Networks

Sanjib Ghosh, Andrzej Opala, Michał Matuszewski, Tomasz Paterek, and Timothy C. H. Liew

*Abstract*— **Reconstructing quantum states is an important task for various emerging quantum technologies. The process of reconstructing the density matrix of a quantum state is known as quantum state tomography. Conventionally, tomography of arbitrary quantum states is challenging as the paradigm of efficient protocols has remained in applying specific techniques for different types of quantum states. Here, we introduce a quantum state tomography platform based on the framework of reservoir computing. It forms a quantum neural network and operates as a comprehensive device for reconstructing an arbitrary quantum state (finite-dimensional or continuous variable). This is achieved with only measuring the average occupation numbers in a single physical setup, without the need of any knowledge of optimum measurement basis or correlation measurements.**

*Index Terms*— **Artificial neural networks, machine intelligence, quantum computing, tomography.**

## I. Introduction

THE interconnectivity of nodes in neural networks allows them to represent data in a high-dimensional effective or feature space, in which they can learn to perform complicated transformations based on examples of the desired output from a given input. Typically, the signal at each node of a neural network is encoded in some analog variables. In a physical implementation, this could represent the action potential of a biological network, the charge of a transistor in an electronic system, or the amplitude of light in an optical network.

In systems where the physical size of a network node is small, comparable to the de Broglie wavelength, the laws of quantum physics come into play. The state of each node is no longer characterized by a single analog variable but by a quantum state residing in the Hilbert space. Effectively, the Hilbert space allows the traditional feature space of a neural network to become exponentially larger. Consequently, quantum neural networks [1] show speed-up of both learning [2], [3] and (theoretically) problem solving efficiency [4]–[7]. However, as the systems for building such networks typically require nanoscale precision to engineer correctly the couplings between network nodes, they are not easy to come by. If such controllability can be achieved, then quantum neural networks are powerful architectures, which can enhance quantum computers [8], [9] and quantum annealers [10]. Yet, since there is only limited access to even small-scale quantum computers, many applications of quantum neural networks are unexplored. The majority of works focus on how quantum systems can be used for classical tasks; however, they could also be applicable to tasks in quantum information processing, i.e., tasks that are not only enhanced by the availability of the Hilbert space but cannot be performed without the Hilbert space to begin with.

Among the forms of classical recurrent neural networks, reservoir computing emerged as particularly suitable for hardware implementations in a wide variety of systems [11]. The training of recurrent neural networks is often computationally inefficient and can be a nonconverging process [12], [13]. In contrast, reservoir computing uses a randomly connected reservoir as a processing unit where the input signal is to be fed. Training takes place only at the readout level and keeps the reservoir itself unchanged. Consequently, training of a classical reservoir computer is relatively straightforward and computationally efficient [12]. The concept was recently generalized to quantum systems and shown to allow the classification of quantum states as entangled or separable [14] (entanglement is a property of quantum states empowering communication and computation). While recognizing entanglement is an important task in quantum information, it is far from a complete characterization of a quantum state. While in classical physics, a state is determined by measuring some set of characteristic quantities (e.g., the number of particles or intensity in each mode) that should be the same if the same measurement is performed on identical states, in quantum physics, a state does not have well-defined characteristics before measurement, and measurements performed on identical states can have different results. A quantum state is, thus, defined by a distribution of different possible measurement outcomes, and the possible correlations between those measurements. The most general quantum state is typically represented by a density matrix, and the process of reconstructing this density

Manuscript received March 2, 2020; revised June 1, 2020; accepted July 11, 2020. Date of publication July 31, 2020; date of current version July 7, 2021. This work was supported in part by the Singapore Ministry of Education Academic Research Fund Tier 2 under Project MOE2015-T2-2-034, Project MOE2017-T2-1-001, and Project MOE2019-T2-1-004. The work of Andrzej Opala and Michał Matuszewski was supported by the National Science Center, Poland, under Grant 2016/22/E/ST3/00045. *(Corresponding author: Sanjib Ghosh.)*

Sanjib Ghosh is with the School of Physical and Mathematical Sciences, Nanyang Technological University, Singapore 637371 (e-mail: sanjibghosh87@u.nus.edu).

Andrzej Opala and Michał Matuszewski are with the Institute of Physics, Polish Academy of Sciences, 02-668 Warsaw, Poland.

Tomasz Paterek is with the School of Physical and Mathematical Sciences, Nanyang Technological University, Singapore 637371, and also with the Faculty of Mathematics, Physics and Informatics, Institute of Theoretical Physics and Astrophysics, University of Gdańsk, 80-308 Gdańsk, Poland.

Timothy C. H. Liew is with the School of Physical and Mathematical Sciences, Nanyang Technological University, Singapore 637371.

This article has supplementary downloadable material available at https://ieeexplore.ieee.org, provided by the authors.

Color versions of one or more of the figures in this article are available online at https://ieeexplore.ieee.org.

Digital Object Identifier 10.1109/TNNLS.2020.3009716

matrix from multiple copies of a quantum state is known as quantum state tomography. Whether with finite-dimensional or continuous variable systems, quantum state tomography requires the processing of outcomes (complex data) of measurements in a complete set of bases [15]–[19]. The number of required measurement bases increases exponentially with the increasing size of a quantum system (e.g., number of qubits or number of quantum modes). Noting that performing measurements in different bases amounts to reconfiguring an experimental setup, quantum state tomography becomes exceedingly challenging as the number of measurement bases grows. While adaptive and self-guided methods [20]–[22] and neural network protocols used on classical data obtained from independent experiments [23]–[25] or methods taking advantage of specific properties of finite-dimensional density matrices [26], [27] reduce the number of required measurement bases, they still need many measurements in different bases to fully reconstruct quantum states. Protocols based on a many-outcome measurement do avoid multiple reconfigurable measurements [28], [29]; however, complexity remains in single-photon detections, their correlation measurements, and in the reconstruction method that depends on the specific transformation used in the experiment. Advanced tomographic schemes in the continuous variable domain, e.g., schemes based on measurements on the displaced quantum states [30] or via a Lagrange interpolation method [31], also require measurements in different bases in phase space. Moreover, none of these schemes are universally applicable for states representing both finite-dimensional and continuous-variable systems.

Here, we present quantum reservoir state tomography (QRST) as a platform for universal quantum state reconstruction. We consider a device that receives quantum information in the form of an optical field, which merges into a quantum reservoir network. The readout elements of the device are then provided by the occupation numbers measured on the reservoir (see the scheme in Fig. 1) rather than requiring any correlation measurements. This scheme constitutes a quantum version of reservoir computing that performs a quantum task but here without assuming the preexistence of a quantum computer. For QRST, while the quantum features of a reservoir allow simplifying the experimental protocol to a single measurement process, its reservoir computing framework enables to simplify the reconstruction subsequent to the measurement and guarantees its universal success for any quantum states in finite-dimensional and continuous-variable domains.

## II. Results

Our scheme of quantum tomography using a quantum reservoir is schematically described in Fig. 1, where an input quantum state, represented by the density matrix $\rho_{\text{in}}$, is incident on a quantum network excited with a uniform coherent field $P$. We consider a 2-D lattice of quantum dots (two-level systems) for the quantum network (reservoir), represented by the Hamiltonian

$$\hat{H} = \sum_{\langle ij \rangle} J_{ij}\left(\hat{c}_i^\dagger \hat{c}_j + \hat{c}_j^\dagger \hat{c}_i\right) + P \sum_i \left(\hat{c}_i^\dagger + \hat{c}_i\right) \tag{1}$$

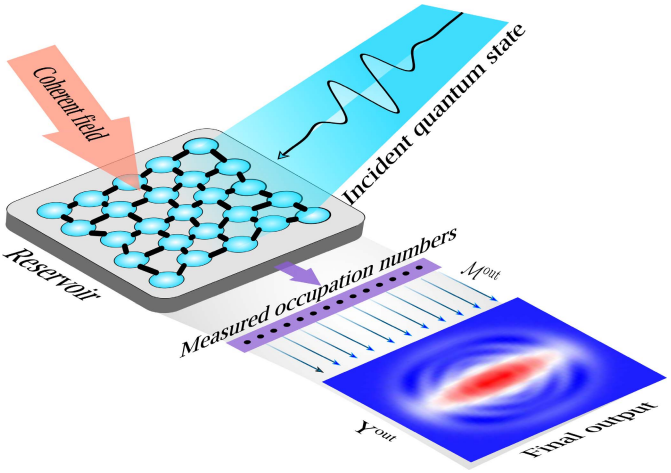


Fig. 1. Scheme of QRST. Here, the reservoir is a fermionic lattice with random intersite couplings. The input quantum state is taken in the form of an optical field incident on the reservoir. The incident field is coupled to the reservoir in cascade. The reservoir is excited with an additional resonant pump. The occupation numbers of the fermionic sites provide the readout elements, which then yield the final output $\mathbf{Y}^{\text{out}}$ in the form of the reconstructed density matrices or the Wigner functions. The output weight matrix $\mathcal{M}^{\text{out}}$ is to be obtained through training.

where $\hat{c}_i$ is the fermionic field operator (represents the quantum dots) at site $i$, and $J_{ij}$ are the hopping amplitudes between the nearest neighbor sites $i$ and $j$. We consider that $J_{ij}$ are randomly distributed between positive and negative values such that the spectral radius (largest absolute eigenvalue) of the hopping part of the Hamiltonian is $\tilde{J}$. The dynamics of the system can be described by the quantum master equation

$$i\hbar\dot{\rho} = [\hat{H}, \rho] + \frac{i\gamma}{2}\sum_j \mathcal{L}(\hat{c}_j) + i\Theta(t-t_1)\sum_k \frac{\eta_k}{2\gamma}\mathcal{L}(\hat{a}_k) + i\Theta(t-t_1)\sum_{k,j}\mathcal{M}_{jk}^{\text{in}}\left(\left[\hat{a}_k\rho, \hat{c}_j^\dagger\right] + \left[\hat{c}_j, \rho\hat{a}_k^\dagger\right]\right) \tag{2}$$

where $\hat{a}_k$ are the field operators of the input modes (which can be bosons or fermions), $\rho$ is the combined density matrix representing the reservoir and the input modes, and $\mathcal{L}(\hat{x}) = 2\hat{x}\rho\hat{x}^\dagger - \hat{x}^\dagger\hat{x}\rho - \rho\hat{x}^\dagger\hat{x}$ is the Lindblad superoperator for a field operator $\hat{x}$. On the right-hand side of (2), the first term represents the coherent Hamiltonian evolution of the reservoir, the second term represents the decay in the reservoir modes with the rate $\gamma/\hbar$, and the third term is representing decay in the input modes with rates $\eta_k/(\hbar\gamma)$ due to the cascaded coupling between the input modes and the reservoir, represented by the remaining terms [32], [33]. The parameters $\eta_k = \sum_j (\mathcal{M}_{jk}^{\text{in}})^2$ are set by the cascaded formalism to ensure that the emitted photons from the input modes are only absorbed by the reservoir. $\mathcal{M}_{jk}^{\text{in}}$ are the input weights randomly chosen from the interval $[0, \omega]$. $\Theta(t-t_1)$ is the Heaviside function signifying that the cascaded coupling between the input modes and the reservoir fermions starts at $t = t_1$, where $t_1$ is an initial time interval.

We perform QRST in four steps.

1) Initially, for $0 \le t < t_1$, the reservoir is only excited with the uniform field $P$ such that the reservoir at time $t_1$ reaches a steady state.

2) Then, we activate the cascaded coupling between the input modes and the reservoir through the Heaviside function. This coupling moves the reservoir out of its initial steady state.
3) In this transient, we measure the expectation values of the occupation numbers $n_j = \langle \hat{c}_j^\dagger \hat{c}_j \rangle$ at time $t = t_1 + \tau$ for all fermions in the reservoir. These occupation numbers provide the readout elements for the processing.
4) We evaluate the desired output $\mathbf{Y}^{\text{out}} = \mathcal{M}^{\text{out}}\vec{n} + \vec{m}$ from the readout elements, where the output weight matrix $\mathcal{M}^{\text{out}}$ and state-independent constant vector $\vec{m}$ are to be determined through training.

We first present the results of simulations of this tomographic scheme in various situations to demonstrate its universality and then explain the observed features with a mathematical proof of the process.

### A. Tomography in Finite Dimensions

Consider a system represented by a $D$ dimensional Hilbert space. The density matrices representing the quantum states of this system can be written as

$$\rho_{\text{in}} = \frac{1}{D}\left(\mathbb{1} + \sum_i s_i \zeta_i\right) \tag{3}$$

where $s_i$ are the $D^2 - 1$ independent parameters required to describe a state in $D$ dimensions, and $\zeta_i$ are the SU(D) generators that together with the identity matrix $\mathbb{1}$ satisfy the completeness relation in the space of $D \times D$ matrices [34]. The parameters $s_i$ are chosen using the Monte Carlo sampling technique with the constraint that all eigenvalues of $\rho_{\text{in}}$ are positive semidefinite (see the Supplementary Material). To perform tomography, we assign $\mathbf{Y}^{\text{out}} = \vec{\rho}_{\text{in}}$, where $\vec{\rho}_{\text{in}}$ represents the density matrix $\rho_{\text{in}}$ arranged in a column vector format. We find the output weight matrix $\mathcal{M}^{\text{out}}$ and the constant vector $\vec{m}$ by training the network with known examples of random density matrices. Here, training is equivalent to solving the matrix equation $\vec{\rho}_{\text{in}} = \mathcal{M}^{\text{out}}\vec{n} + \vec{m}$. As the matrix equation corresponds to $D^2$ linear equations, the required minimum number of known examples of $\rho_{\text{in}}$ is $D^2$ for $D$ dimensional states. These training states require to be linearly independent such that each example represents an independent equation. In fact, we can consider $D^2$ number of randomly generated states for training, as it is statistically unlikely to randomly generate linearly dependent states. However, we train the network using the ridge regression technique [12] with slightly larger number of examples than $D^2$ to avoid insufficient number of independent equations due to the rare generation of linearly dependent states. Once $\mathcal{M}^{\text{out}}$ and $\vec{m}$ are determined, the density matrix of an input state is reconstructed from the output as $\vec{\rho}_{\text{in}}^{\text{tomo}} = \mathbf{Y}^{\text{out}} = \mathcal{M}^{\text{out}}\vec{n} + \vec{m}$, where $\vec{\rho}_{\text{in}}^{\text{tomo}}$ is the vector form of the reconstructed density matrix $\rho_{\text{in}}^{\text{tomo}}$. This reconstructed matrix $\rho_{\text{in}}^{\text{tomo}}$ might be imprecise. To estimate possible errors in the tomography, we calculate the fidelity

$$F = \left(\text{Tr}\left[\sqrt{\sqrt{\rho_{\text{in}}}\,\rho_{\text{in}}^{\text{tomo}}\,\sqrt{\rho_{\text{in}}}}\right]\right)^2. \tag{4}$$

In error-free tomography, $F = 1$, and $F < 1$ otherwise.

In Fig. 2(a), we show the fidelity $F$ for different reservoir sizes $N$ and dimensions $D$. The fidelity systematically increases with increasing reservoir size for any $D$, and the fidelity reaches 1 at $N = D^2 - 1$ for $D = 2$ and 3, respectively. We could not fully verify this relation for $D = 4$ as it requires to simulate a quantum reservoir of size $N = 15$, which is beyond our computational reach. However, we introduce the concept of "time multiplexing" in Section II-C, which drastically reduces the required size $N$.

### B. Typical State Tomography

We have shown the tomography of density matrices sampled in the full $D^2 - 1$ parameter space. However, quantum states generated in actual experiments are often restricted in a small subspace of the full parameter space. As an example for representing such states, we consider noisy Bell states: $\rho_{\text{in}} = (1 - \epsilon)|\psi\rangle\langle\psi| + (\epsilon/4)\mathbb{1}$, where $|\psi\rangle = (|00\rangle + e^{-i\varphi}|11\rangle)/\sqrt{2}$, and $\epsilon$ is a parameter quantifying the amount of noise. For training, we use a supervised learning technique that requires example input states. We generate the example states $\rho_{\text{in}}$ with randomly chosen $\epsilon$ and $\varphi$ from the intervals $[0, 0.2]$ and $[0, 2\pi]$, respectively. Using the ridge regression method and the example states, we obtain the output weight matrix $\mathcal{M}^{\text{out}}$ and $\vec{m}$ (see the Supplementary Material). After the training, we use another set of randomly generated $\epsilon$ and $\varphi$ to obtain the corresponding $\rho_{\text{in}}$ for testing the reconstruction ability of QRST. While the full reconstruction of an arbitrary two-qubit density matrix requires 15 readout elements, full reconstruction of the noisy Bell states requires only two readout elements [see Fig. 2(a)]. This reduction in the required number of readout elements is due to the smaller number of independent parameters needed to represent the input states (training and testing are performed with the same class of states). Similar reasons manifest in the tomography of low-rank density matrices [26] or in adaptive methods [22]. However, QRST automatically learns this fact from training and applies it for tomography without any state-specific modification in the scheme.

### C. Time Multiplexing

The abovementioned simulations show that a single measurement process (measuring average occupation numbers in a single physical setup) with a reservoir size $N = D^2 - 1$, which provides $D^2 - 1$ readout elements, is sufficient for full reconstruction of density matrices. However, note that one can increase the number of readout elements by performing measurements at multiple times. The input modes are coupled to the reservoir for a time interval $\tau$ between $t = t_1$ and $t = t_1 + \tau$. One can measure the occupation numbers at $M$ different times $t = t_1 + j\tau/M$ $(j = 1, 2, \ldots, M)$ during this time interval. Now, instead of $N$ readout elements in a reservoir size of $N$, one has $N \times M$ readout elements and, thus, the expected reservoir size $N = (D^2 - 1)/M$ to achieve a fidelity $F = 1$. In Fig. 2(b)–(d), we show the fidelity of the reconstructed density matrices as functions of the reservoir size $N$ and multiplexity $M$ that indeed confirms this scaling. In Fig. 2(e) and (f), we show an example of a two-qubit density

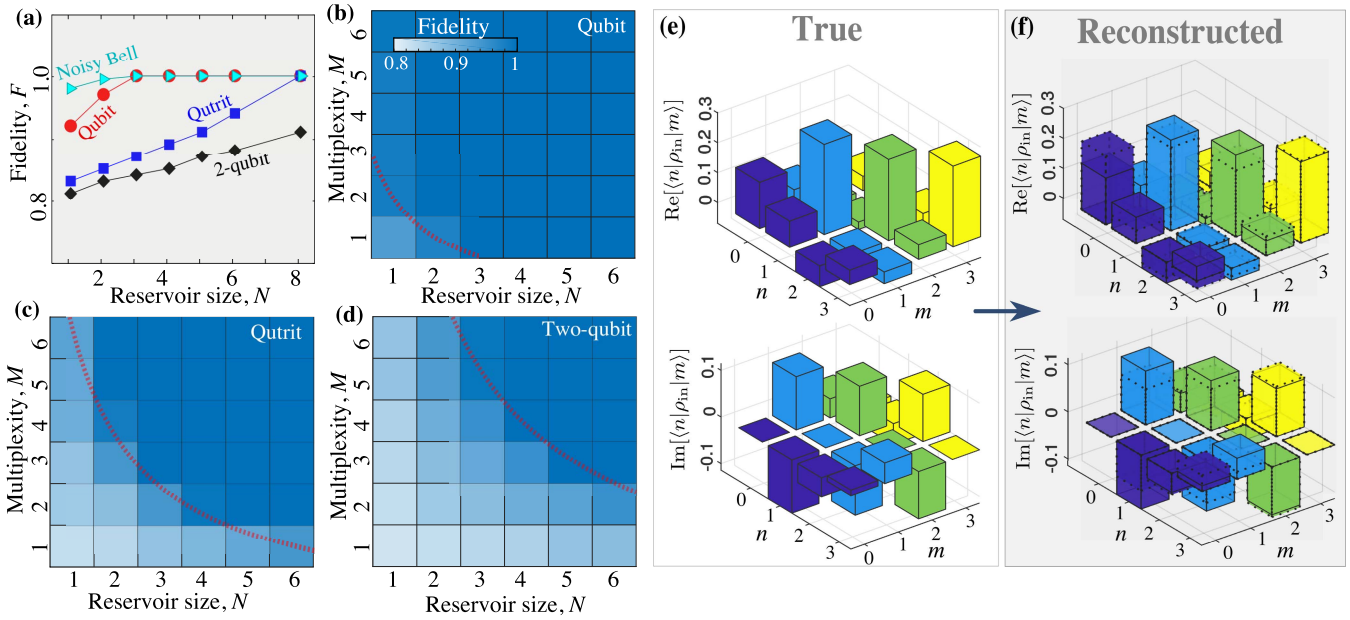


Fig. 2. (a) Calculated fidelities as functions of reservoir size $N$ (number of fermions) for qubit, qutrit, two-qubit, and noisy Bell states. Color plots of fidelities calculated for (b) qubits, (c) qutrits, and (d) two-qubit as functions of reservoir size $N$ and measurement multiplexity $M$ (the number of time instances when the occupation numbers are measured). The red dotted lines in each of the plots represent the relation $NM = D^2 - 1$. We find full tomographic reconstruction of the density matrices with fidelity $F = 1$ for the regimes beyond the red dotted lines where $NM \geq D^2 - 1$. The data points are averaged over ten realizations of all random parameters. (e) and (f) Real and imaginary parts of an example two-qubit density matrix and the corresponding reconstruction by a QRST device with $N = 2$, $M = 6$ (dotted line) and $N = 6$, $M = 6$ (solid line) with the fidelities $0.9515 \pm 10^{-5}$ and $1 \pm 10^{-5}$, respectively. The basis states $|n\rangle$ for $n = 0, 1, 2$, and 3 (same for $m$) represent the two-qubit basis states $|00\rangle$, $|01\rangle$, $|10\rangle$, and $|11\rangle$, respectively. Here, we use $\tilde{J}/\gamma = 1$, $\omega/\gamma = 1$, $t_1 = 7.6\hbar/\gamma$, $\tau = 1.5\hbar/\gamma$, and $P/\gamma = 0.3$, and the random parameters $\epsilon$ and $\varphi$ are chosen from the intervals $[0,\ 0.2]$ and $[0, 2\pi]$, respectively.

matrix and the corresponding reconstructions using ($N = 2$ and $M = 6$) and ($N = 6$ and $M = 6$).

### *D. Continuous Variable Tomography*

We now consider continuous variable tomography using QRST. Despite an infinite (large) dimensionality of a continuous variable state, we show that an accurate tomography can be performed with a few readout elements in a single measurement process. For continuous variable states, it is convenient to represent them with the Wigner functions $W(\rho_{\text{in}}; x_i, p_j)$, which are defined on a grid of continuous variables $x_i$ and $p_j$ for a given density matrix $\rho_{\text{in}}$. We assign $Y_{ij}^{\text{out}} = W(\rho_{\text{in}}, x_i, p_j)$ as the output for QRST. Training provides the optimum output weight matrix and constants such that the reconstructed $W(\rho_{\text{in}}; x_i, p_j) = \sum_k \mathcal{M}_{ijk}^{\text{out}} n_k + m_{ij}$ has the minimum deviation from the corresponding known training Wigner functions. We use 96 randomly generated squeezed-thermal states for training. In Fig. 3, we show the reconstructed Wigner functions of some randomly generated squeezed-thermal states (see the Supplementary Material) with a reservoir size of $N = 4$ and a multiplexity of $M = 4$ and their deviations from the true Wigner functions. As a quantitative measure of the tomography error, we define

$$E = \sqrt{\frac{\sum_{i,j}[W(\rho_{\text{in}}; x_i, p_j) - W^{\text{tomo}}(\rho_{\text{in}}; x_i, p_j)]^2}{\sum_{i,j}[W(\rho_{\text{in}}; x_i, p_j) + W^{\text{tomo}}(\rho_{\text{in}}; x_i, p_j)]^2}} \tag{5}$$

where $W^{\text{tomo}}(\rho_{\text{in}}; x_i, p_j)$ is the reconstructed Wigner function corresponding to the true one $W(\rho_{\text{in}}; x_i, p_j)$. In Fig. 4, we show the histogram of the estimated errors for different

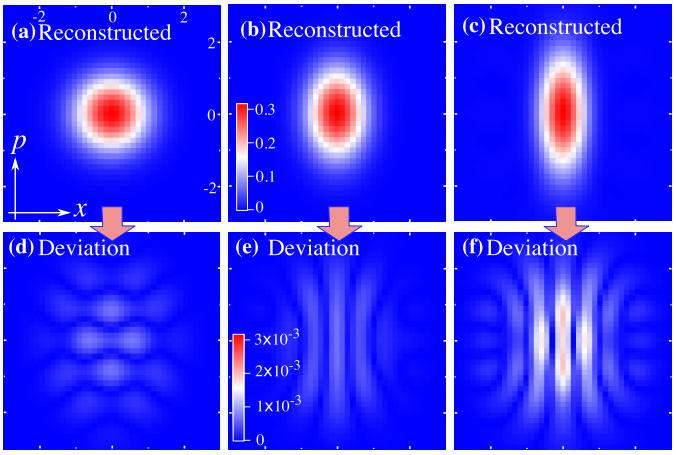


Fig. 3. Tomography of continuous variable quantum states. Here, we show some considered examples of (a)–(c) reconstructed squeezed-thermal states and (d)–(f) their deviations from the true states. The deviation is defined by $|W(\rho_{\text{in}}; x_i, p_j) - W^{\text{tomo}}(\rho_{\text{in}}; x_i, p_j)|$. Color scales for (a)–(c) and (d)–(f) are given in (b) and (e), respectively. We here use 16 readout elements ($N = 4$, $M = 4$), $\tilde{J}/\gamma = 1$, $\omega/\gamma = 1$, $t_1 = 7.6\hbar/\gamma$, $\tau = 1.5\hbar/\gamma$, and $P/\gamma = 0.3$.

numbers of readout elements. We find the error systematically decreases with an increasing number of readout elements. In fact, the error is impressively low even with a small reservoir size, such as $N = 4$ with $M = 4$. Note that the effective dimension $D$ of the considered squeezed-thermal states is large. We identify the effective dimension $D$ as the smallest dimension for which the mean photon number becomes independent of $D$ (see the Supplementary Material).

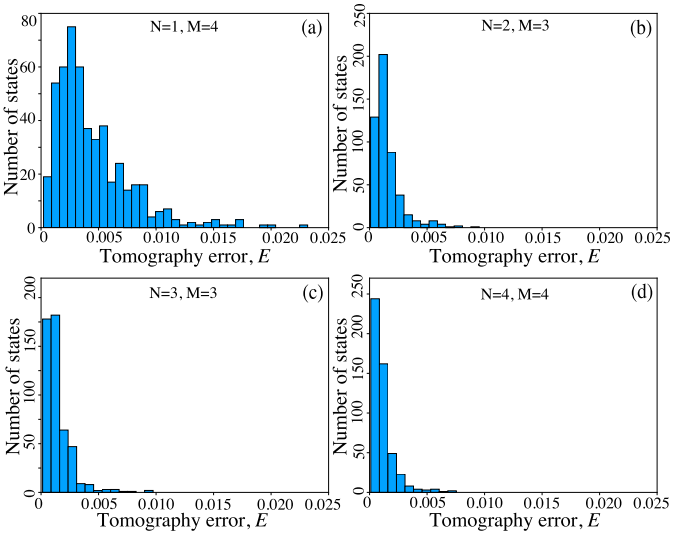


Fig. 4. Histograms for errors in estimating Wigner functions for increasing number of readout elements. (a)–(d) Histogram of 500 squeezed-thermal states for their tomographic errors $E$ defined in (5). The considered number of readout elements are 4, 6, 9, and 16 for (a)–(d), respectively. Here, we use $\bar{J}/\gamma = 1$, $\omega/\gamma = 1$, $t_1 = 7.6\hbar/\gamma$, $\tau = 1.5\hbar/\gamma$, and $P/\gamma = 0.3$.

As shown in Fig. 3, this small reservoir can reconstruct well the features of the Wigner functions. Already, for a reservoir with $N = 3$ and $M = 3$, which is an even smaller reservoir with little multiplexity, the reconstruction errors are mostly close to zero. This demonstrates that QRST is a very powerful tool for quantum state tomography in the continuous variable domain.

## III. Theoretical Generalization

Let us now explain the features observed in the simulations and prove their generalization to arbitrary dimension. Since there are $D^2 - 1$ independent real parameters in a density matrix in order to estimate all of them, the reservoir must have at least $N = D^2 - 1$ lattice sites (or $N = (D^2 - 1)/M$ if time-multiplexing is used). In the numerics, we find that for this number of sites QRST trained with $D^2$ random states reconstructs an arbitrary input state perfectly, i.e. with unit fidelity. This can be understood as follows. Note that an arbitrary density matrix can be decomposed in terms of $D^2$ linearly independent states

$$\rho_{\text{in}} = \sum_i \alpha_i \rho_i, \quad \text{with} \quad \sum_i \alpha_i = 1 \tag{6}$$

where the coefficients $\alpha_i$ are not necessarily nonnegative but sum up to unity due to normalization. A random set of $D^2$ states is practically always linearly independent. Therefore, training of QRST with random states $\rho_i$ is equivalent to determining the matrix $\mathcal{M}^{\text{out}}$ and vector of constants $\vec{m}$ by solving the following set of $D^2$ linear equations:

$$\mathcal{M}^{\text{out}}\vec{n}_i + \vec{m} = \vec{\rho}_i \tag{7}$$

where $\vec{n}_i$ is the vector of readout elements for random input state $\rho_i$ with vector representation $\vec{\rho}_i$. In the Supplementary Material, we prove that the mean occupation number of a fermionic site of the reservoir can be represented as a positive-operator-valued measure (POVM) measurement on the input modes

$$n_j = \langle \hat{c}_j^\dagger \hat{c}_j \rangle = \text{tr}(\rho_{\text{in}} E_j) \tag{8}$$

where $E_j$ is the POVM element corresponding to finding a fermion on the $j$th lattice site. Hence, the vector of readout elements corresponding to the arbitrary state in (6) is given by $\vec{n} = \sum_i \alpha_i \vec{n}_i$. It is now essential that our reconstruction procedure trained in (7) is a linear map on the readout vector $\vec{n}$. Indeed, one readily verifies that $\mathcal{M}^{\text{out}}\vec{n} + \vec{m} = \vec{\rho}_{\text{in}}$, i.e., QRST perfectly recovers an arbitrary input state.

In conventional quantum state tomography, each von Neumann measurement basis provides at most $D - 1$ independent real parameters characterizing the input state. Accordingly, one needs at least $D + 1$ such measurement bases to reconstruct an arbitrary state in the $D$-dimensional Hilbert space [35]. Typically, more measurement bases are required due to the complexity of these $D + 1$ measurements as they necessarily require projections on entangled states [36]. A way to reduce the number of measurement bases is to consider their generalization in the form of informationally complete POVMs. Typically, these are also difficult to implement (see [37]–[39]), and it is our main point here that the informationally complete set of $N$ POVMs that we propose is practically implementable even for high-dimensional input. Furthermore, an experimenter does not have to know the corresponding POVM elements. They are established indirectly via training, and the output of QRST is the final density matrix.

## IV. Error Analysis

As in any tomography scheme, the presence of measurement errors can introduce limitations. In a given run of the experiment, the measurement of the occupation number of a given node would give an integer number of particles. It is only by repeating the experiment multiple times that an average is obtained. The error in the measured occupation number is then given by

$$\sigma_{\overline{n}_j} = \sigma_{n_j}/\sqrt{N_r} \tag{9}$$

where $N_r$ is the number of repetitions and $\sigma_{n_j} = (\langle \hat{n}_j^2 \rangle - \langle \hat{n}_j \rangle^2)^{1/2}$ is the standard deviation in the particle number, which could be obtained from the density matrix. In addition to the quantum error, we also consider other random and systematic errors in the experimental setup.

To characterize the possibility of further random errors, we consider that even after being repeated $N_r$ times, the evaluation of the occupation numbers with a given input state $\rho_{\text{in}}^{(i)}$ would still contain an error, where the actual value of the average occupation number is

$$\tilde{n}_j = n_j(1 + \sigma_r g_{r,i,j}) \tag{10}$$

where $g_{r,i,j}$ is a Gaussian random variable, which is different for different input states. $\sigma_r$ defines the overall size of the random errors, and we allow it to be larger than the quantum error, potentially characterizing additional random errors in an experimental setup. In Fig. 5(a), we show how the average

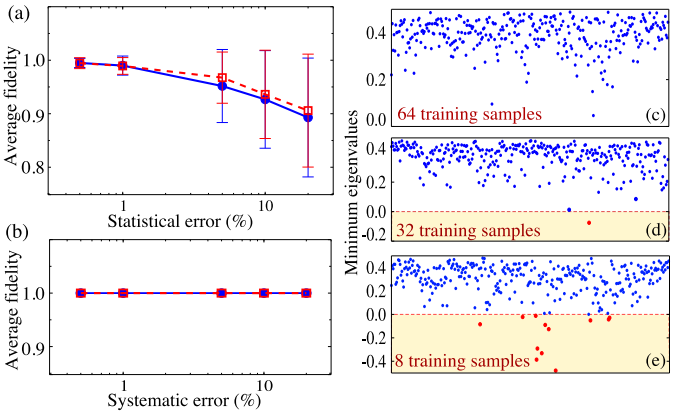


Fig. 5. Effects of (a) statistical errors and (b) systematic errors in QRST returning states of a single qubit. We plot the average fidelity (averaged over 160 random qubit states) for two reservoir sizes $N = 3$ (blue solid line) and $N = 4$ (red dotted line). The statistical and systematic error percentages are given by $\sigma_r \times 100\%$ and $\sigma_s \times 100\%$, respectively. (c)–(e) Minimum eigenvalues of 320 reconstructed density matrices for the number of training samples 64, 32, and 8, respectively. The positive and negative eigenvalues are indicated with blue and red points. Here, we considered 20% statistical and systematic errors both and a reservoir of size $N = 3$. We find that even with high errors in the output, the reconstructed density matrices show negative eigenvalues only rarely for a small number of training samples.

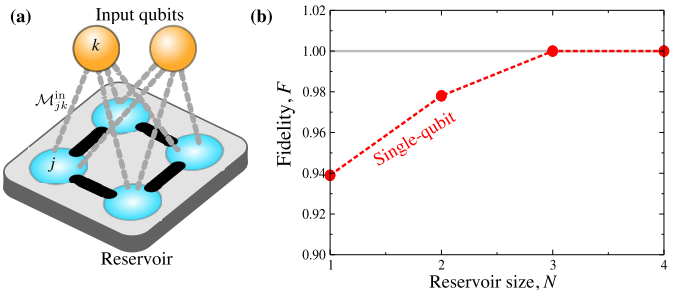


Fig. 6. Quantum state tomography with alternative form of coupling between the input mode and the reservoir sites. (a) Schematic of the coupling between input qubits and the reservoir using quantum hopping. (b) Calculated fidelities as functions of reservoir size $N$ (with $M = 1$) for single-qubit states. Other parameters are taken same, as mentioned in Fig. 2.

fidelity of single-qubit states varies with the overall size of the random errors. Even with errors on the order of 10%, the fidelity remains above 90%. Furthermore, the use of a larger reservoir allows for a slight compensation of errors, and we can recall that random errors in an experimental setup could be further reduced by repeating the experiment more times.

Systematic errors in the average occupation numbers can be accounted for by defining

$$\tilde{n}_j = n_j(1 + \sigma_s g_{s,j}) \tag{11}$$

where $\sigma_s$ defines the size of the systematic errors that are given by a Gaussian distribution and taken different for each node, independent of the input state. As shown in Fig. 5(b), the fidelity is unaffected by systematic errors. This is because, provided that the systematic error is accounted for both in training and testing, the network would have learned to compensate for the systematic errors in measurement. Mathematically, this is explained from the relation $\mathcal{M}^{\text{out}}(\vec{n}_i + \delta\vec{n}) + \vec{m} = \vec{\rho}_i$, where the systematic error $\delta n_j = \sigma_s g_{s,j} n_j$ is independent of the input state index $i$. Thus, we can redefine the vector $\vec{m}' = \vec{m} + \mathcal{M}^{\text{out}}\delta\vec{n}$ to write $\mathcal{M}^{\text{out}}\vec{n}_i + \vec{m}' = \vec{\rho}_i$, where $\vec{m}'$ remains a constant vector that does not depend on the input state and is determined by training.

The right figures in Fig. 5 show the minimum eigenvalues of the reconstructed density matrices. We find that for sufficient training, the eigenvalues of the reconstructed density matrix are nonnegative even when the output errors are as large as 20%. Although we have not explicitly imposed positivity on the reconstructed density matrix, the training process, which is performed only with physical density matrices, drives the neural network to form only a positive density matrix at the output. However, practical limitations, such as an insufficient number of training samples or extremely small reservoir size together with large measurement error, can lead to the loss of positivity of the estimated density matrix [see Fig. 5(e)]. In such situations, a maximum likelihood estimation can be employed to find out the closest physical density matrix. A wealth of study has been devoted to explore this estimation [40]–[44]. When needed, these methods can directly be applied as a final step in the QRST scheme. We emphasize again that our results strongly suggest that nonphysical reconstructions do not arise for a sufficiently large number of training samples, and note that the training has to be performed only once.

## V. Discussion

For hardware implementation, our proposed platform can be realized in a wide range of systems in principle, e.g., arrays of semiconductor quantum dots, coupled superconducting qubits, and trapped ions and atoms. Here, we have considered a cascade formalism to model the coupling between the optical input states to the reservoir sites. Equivalently, for qubits realized in ions, atoms, spins, and superconductors, the cascade coupling can be replaced with quantum hopping (Josephson type tunneling) between the input qubits and the reservoir sites. This can be described by an interaction Hamiltonian

$$\hat{H}_{\text{int}} = \sum_{jk} \mathcal{M}^{\text{in}}_{jk}\left(\hat{c}_j^\dagger \hat{a}_k + \hat{a}_k^\dagger \hat{c}_j\right) \tag{12}$$

where the whole system is described by the total Hamiltonian $\hat{H}_{\text{tot}} = \hat{H} + \Theta(t - t_1)\hat{H}_{\text{int}}$. For spin systems, the same interaction Hamiltonian is applicable. In the language of spins, $\hat{H}_{\text{int}}$ translates to $\hat{H}_{\text{int}} = \sum_{jk} \mathcal{M}^{\text{in}}_{jk}(\hat{\sigma}_j^+\hat{\sigma}_k^- + \hat{\sigma}_k^+\hat{\sigma}_j^-)$, where the correspondence is made with $(\hat{c}_j, \hat{c}_j^\dagger) \rightarrow (\hat{\sigma}_j^-, \hat{\sigma}_j^+)$ and $(\hat{a}_k, \hat{a}_k^\dagger) \rightarrow (\hat{\sigma}_k^-, \hat{\sigma}_k^+)$, and $\hat{\sigma}_m^\pm = (\hat{\sigma}_m^x \pm i\hat{\sigma}_m^y)/2$ are the Pauli matrices for site $m$. This interaction is also known as the $XY$ interaction between the spins. In Fig. 6, we show that QRST can also be performed by replacing the cascade coupling with $\hat{H}_{\text{int}}$. Exciton–polaritons in semiconducting microcavities (hybrid light–matter quasiparticles) are also suitable for realizing quantum reservoirs as they naturally couple with external optical fields and can reach strongly interacting regimes. Here, the coupling between the input state and the reservoir is realizable either with the cascade method or with the quantum hopping. Moreover, while implementing a quantum reservoir in a physical system, our protocol does not require precise

control on the system parameters, rather the randomness is a useful resource for successful quantum state tomography.

Without time multiplexing, the required reservoir size for $D$ dimensional tomography is $N = D^2 - 1$. With the time multiplexing ($M$), the required size reduces to $N = (D^2 - 1)/M$. An alternative route to reduce $N$ would be measuring the quantum correlations between the nodes. Since the number of possible quantum correlations increases exponentially with $N$, the required reservoir size would decrease to the order of $\log(D)$. However, we think that measuring an exponentially large number of quantum correlations would be a much challenging task compared with measuring the average occupation numbers.

## VI. Conclusion

We have presented QRST as a platform for quantum state reconstruction. Unlike existing schemes for specific quantum states either in the finite-dimensional or continuous-variable domain, our scheme operates the same for any quantum state. Within our scheme, tomography is accomplished with a single measurement process of intensity, which does not require photon number resolution or correlated detection, in contrast to previous tomography schemes that use multiple measurements in different bases and correlation measurements of complex informationally complete generalized measurement schemes. Here, the challenge can be in achieving a reservoir that can be large for higher dimensional tomography. However, we have shown that the required size of a quantum reservoir can be drastically reduced by measuring occupation numbers at the reservoir lattice sites at multiple times (time multiplexing) for readout. It is, thus, an experimentally friendly, practically scalable scheme that can be universally applied to any quantum state.

## Acknowledgment

The authors would like to thank Tanjung Krisnanda for helpful discussions during the preparation of this article.

## References

[1] J. Biamonte, P. Wittek, N. Pancotti, P. Rebentrost, N. Wiebe, and S. Lloyd, "Quantum machine learning," *Nature*, vol. 549, pp. 195–202, Sep. 2017, doi: 10.1038/nature23474.

[2] V. Dunjko, J. M. Taylor, and H. J. Briegel, "Quantum-enhanced machine learning," *Phys. Rev. Lett.*, vol. 117, no. 13, p. 130, Sep. 2016, doi: 10.1103/PhysRevLett.117.130501.

[3] G. D. Paparo, V. Dunjko, A. Makmal, M. A. Martin-Delgado, and H. J. Briegel, "Quantum speedup for active learning agents," *Phys. Rev. X*, vol. 4, no. 3, p. 031, Jul. 2014, doi: 10.1103/PhysRevX.4.031002.

[4] R. Neigovzen, J. L. Neves, R. Sollacher, and S. J. Glaser, "Quantum pattern recognition with liquid-state nuclear magnetic resonance," *Phys. Rev. A, Gen. Phys.*, vol. 79, no. 4, p. 042, Apr. 2009, doi: 10.1103/PhysRevA.79.042321.

[5] M. Benedetti, J. Realpe-Gómez, R. Biswas, and A. Perdomo-Ortiz, "Estimation of effective temperatures in quantum annealers for sampling applications: A case study with possible applications in deep learning," *Phys. Rev. A, Gen. Phys.*, vol. 94, no. 2, p. 022, Aug. 2016, doi: 10.1103/PhysRevA.94.022308.

[6] U. Alvarez-Rodriguez, L. Lamata, P. Escandell-Montero, J. D. Martín-Guerrero, and E. Solano, "Supervised quantum learning without measurements," *Sci. Rep.*, vol. 7, no. 1, p. 13645, Dec. 2017, doi: 10.1038/s41598-017-13378-0.

[7] K. Fujii and K. Nakajima, "Harnessing disordered-ensemble quantum dynamics for machine learning," *Phys. Rev. A, Gen. Phys.pplied*, vol. 8, no. 2, p. 024, Aug. 2017, doi: 10.1103/PhysRevApplied.8.024030.

[8] E. Farhi and H. Neven, "Classification with quantum neural networks on near term processors," 2018, *arXiv:1802.06002*. [Online]. Available: http://arxiv.org/abs/1802.06002

[9] E. Grant *et al.*, "Hierarchical quantum classifiers," *npj Quantum Inf.*, vol. 4, no. 1, p. 65, Dec. 2018, doi: 10.1038/s41534-018-0116-9.

[10] M. H. Amin, E. Andriyash, J. Rolfe, B. Kulchytskyy, and R. Melko, "Quantum Boltzmann machine," *Phys. Rev. X*, vol. 8, no. 2, p. 021, May 2018, doi: 10.1103/PhysRevX.8.021050.

[11] G. Tanaka *et al.*, "Recent advances in physical reservoir computing: A review," *Neural Netw.*, vol. 115, pp. 100–123, Jul. 2019.

[12] M. Lukoševičius, *A Practical Guide to Applying Echo State Networks*, G. Montavon, G. B. Orr, and K.-R. Müller, Eds. Berlin, Germany: Springer, 2012.

[13] Y. Bengio, P. Simard, and P. Frasconi, "Learning long-term dependencies with gradient descent is difficult," *IEEE Trans. Neural Netw.*, vol. 5, no. 2, pp. 157–166, Mar. 1994.

[14] S. Ghosh, A. Opala, M. Matuszewski, T. Paterek, and T. C. H. Liew, "Quantum reservoir processing," *npj Quantum Inf.*, vol. 5, no. 1, p. 35, Dec. 2019, doi: 10.1038/s41534-019-0149-8.

[15] P. J. Shadbolt *et al.*, "Generating, manipulating and measuring entanglement and mixture with a reconfigurable photonic circuit," *Nature Photon.*, vol. 6, pp. 45–49, Dec. 2011, doi: 10.1038/nphoton.2011.283.

[16] A. I. Lvovsky and M. G. Raymer, "Continuous-variable optical quantum-state tomography," *Rev. Modern Phys.*, vol. 81, no. 1, pp. 299–332, Mar. 2009, doi: 10.1103/RevModPhys.81.299.

[17] D. F. V. James, P. G. Kwiat, W. J. Munro, and A. G. White, "Measurement of qubits," *Phys. Rev. A, Gen. Phys.*, vol. 64, no. 5, p. 052, Oct. 2001, doi: 10.1103/PhysRevA.64.052312.

[18] H. Häffner *et al.*, "Scalable multiparticle entanglement of trapped ions," *Nature*, vol. 438, pp. 643–646, Dec. 2005, doi: 10.1038/nature04279.

[19] C.-Y. Lu *et al.*, "Experimental entanglement of six photons in graph states," *Nature Phys.*, vol. 3, pp. 91–95, Jan. 2007, doi: 10.1038/nphys507.

[20] C. Ferrie, "Self-guided quantum tomography," *Phys. Rev. Lett.*, vol. 113, no. 19, p. 190, Nov. 2014, doi: 10.1103/PhysRevLett.113.190404.

[21] R. J. Chapman, C. Ferrie, and A. Peruzzo, "Experimental demonstration of self-guided quantum tomography," *Phys. Rev. Lett.*, vol. 117, no. 4, p. 040, Jul. 2016, doi: 10.1103/PhysRevLett.117.040402.

[22] B. Qi *et al.*, "Adaptive quantum state tomography via linear regression estimation: Theory and two-qubit experiment," *npj Quantum Inf.*, vol. 3, no. 1, p. 19, Dec. 2017, doi: 10.1038/s41534-017-0016-4.

[23] G. Torlai, G. Mazzola, J. Carrasquilla, M. Troyer, R. Melko, and G. Carleo, "Neural-network quantum state tomography," *Nature Phys.*, vol. 14, no. 5, pp. 447–450, May 2018, doi: 10.1038/s41567-018-0048-5.

[24] Y. Quek, S. Fort, and H. Khoon Ng, "Adaptive quantum state tomography with neural networks," 2018, *arXiv:1812.06693*. [Online]. Available: http://arxiv.org/abs/1812.06693

[25] J. Carrasquilla, G. Torlai, R. G. Melko, and L. Aolita, "Reconstructing quantum states with generative models," *Nature Mach. Intell.*, vol. 1, no. 3, pp. 155–161, Mar. 2019, doi: 10.1038/s42256-019-0028-1.

[26] D. Gross, Y.-K. Liu, S. T. Flammia, S. Becker, and J. Eisert, "Quantum state tomography via compressed sensing," *Phys. Rev. Lett.*, vol. 105, no. 15, p. 150, Oct. 2010, doi: 10.1103/PhysRevLett.105.150401.

[27] M. Cramer *et al.*, "Efficient quantum state tomography," *Nature Commun.*, vol. 1, no. 1, p. 149, Dec. 2010, doi: 10.1038/ncomms1147.

[28] D. Oren, M. Mutzafi, Y. C. Eldar, and M. Segev, "Quantum state tomography with a single measurement setup," *Optica*, vol. 4, no. 8, pp. 993–999, 2017. [Online]. Available: http://www.osapublishing.org/optica/abstract.cfm?URI=optica-4-8-993

[29] J. G. Titchener, M. Gräfe, R. Heilmann, A. S. Solntsev, A. Szameit, and A. A. Sukhorukov, "Scalable on-chip quantum state tomography," *npj Quantum Inf.*, vol. 4, no. 1, p. 19, Dec. 2018, doi: 10.1038/s41534-018-0063-5.

[30] M. Hofheinz *et al.*, "Synthesizing arbitrary quantum states in a superconducting resonator," *Nature*, vol. 459, pp. 546–549, May 2009, doi: 10.1038/nature08005.

[31] O. Landon-Cardinal, L. C. G. Govia, and A. A. Clerk, "Quantitative tomography for continuous variable quantum systems," *Phys. Rev. Lett.*, vol. 120, no. 9, p. 090, Mar. 2018, doi: 10.1103/PhysRevLett.120.090501.

[32] H. J. Carmichael, "Quantum trajectory theory for cascaded open systems," *Phys. Rev. Lett.*, vol. 70, no. 15, pp. 2273–2276, Apr. 1993, doi: 10.1103/PhysRevLett.70.2273.

[33] C. W. Gardiner, "Driving a quantum system with the output field from another driven quantum system," *Phys. Rev. Lett.*, vol. 70, no. 15, pp. 2269–2272, Apr. 1993, doi: 10.1103/PhysRevLett.70.2269.

[34] J. Schlienz and G. Mahler, "Description of entanglement," *Phys. Rev. A, Gen. Phys.*, vol. 52, no. 6, pp. 4396–4404, Dec. 1995, doi: 10.1103/PhysRevA.52.4396.

[35] W. K. Wootters and B. D. Fields, "Optimal state-determination by mutually unbiased measurements," *Ann. Phys.*, vol. 191, no. 2, pp. 363–381, May 1989.

[36] M. Wieśniak, T. Paterek, and A. Zeilinger, "Entanglement in mutually unbiased bases," *New J. Phys.*, vol. 13, no. 5, May 2011, Art. no. 053047.

[37] J. Rehacek, B.-G. Englert, and D. Kaszlikowski, "Minimal qubit tomography," *Phys. Rev. A, Gen. Phys.*, vol. 70, no. 5, Nov. 2004, Art. no. 052321.

[38] H. Zhu, Y. S. Teo, and B.-G. Englert, "Two-qubit symmetric informationally complete positive-operator-valued measures," *Phys. Rev. A, Gen. Phys.*, vol. 82, no. 4, Oct. 2010, Art. no. 042308.

[39] A. Kalev, J. Shang, and B.-G. Englert, "Experimental proposal for symmetric minimal two-qubit state tomography," *Phys. Rev. A, Gen. Phys.*, vol. 85, no. 5, May 2012, Art. no. 052115.

[40] K. Banaszek, G. M. D'Ariano, M. G. A. Paris, and M. F. Sacchi, "Maximum-likelihood estimation of the density matrix," *Phys. Rev. A, Gen. Phys.*, vol. 61, no. 1, p. 010, Dec. 1999, doi: 10.1103/PhysRevA.61.010304.

[41] B. Qi, Z. Hou, L. Li, D. Dong, G. Xiang, and G. Guo, "Quantum state tomography via linear regression estimation," *Sci. Rep.*, vol. 3, no. 1, p. 3496, Dec. 2013, doi: 10.1038/srep03496.

[42] J. Shang, Z. Zhang, and H. K. Ng, "Superfast maximum-likelihood reconstruction for quantum tomography," *Phys. Rev. A, Gen. Phys.*, vol. 95, no. 6, p. 062, Jun. 2017, doi: 10.1103/PhysRevA.95.062336.

[43] T. L. Scholten and R. Blume-Kohout, "Behavior of the maximum likelihood in quantum state tomography," *New J. Phys.*, vol. 20, no. 2, Feb. 2018, Art. no. 023050, doi: 10.1088/1367-2630/aaa7e2.

[44] A. Acharya, T. Kypraios, and M. Guţă, "A comparative study of estimation methods in quantum tomography," *J. Phys. A, Math. Theor.*, vol. 52, no. 23, Jun. 2019, Art. no. 234001, doi: 10.1088/1751-8121/ab1958.

**Sanjib Ghosh** was born in India. He received the Ph.D. degree in physics from the National University of Singapore, Singapore, in 2017.

His Ph.D. research was partly conducted at the Kastler–Brossel Laboratory, Paris, France. He is currently a Research Fellow (post-doc) with Nanyang Technological University, Singapore. His research focuses on the theoretical side of quantum optics, neural networks, quantum effects in exciton–polaritons, and the effects of disorder in superconductors and cold atoms.

**Andrzej Opala** received the B.Eng. and M.Sc. degrees in technical physics with nanoengineering specialization from the Wrocław University of Science and Technology, Wrocław, Poland in 2015 and 2017, respectively. He is currently pursuing the Ph.D. degree with the Institute of Physics, Polish Academy of Sciences Warsaw, Poland.

His research interests include light–matter interaction, condensed matter physics, nonlinear physics, and neuromorphic computing systems. Recently, his works focused on exploring the exciton–polaritons systems as a novel platform for neuromorphic computing.

**Michał Matuszewski** received the Ph.D. degree in theoretical physics from the University of Warsaw, Warsaw, Poland, in 2007.

He held a post-doctoral position at The Australian National University, Canberra ACT, Australia, for three years. In 2010, he returned to Warsaw where he established a polariton theory group. He is currently an Associate Professor with the Institute of Physics, Polish Academy of Sciences, Warsaw. His interests include nonlinear phenomena in semiconductor exciton–polariton systems and quantum fluids and optical neural networks.

**Tomasz Paterek** was born in Poland. He received the Ph.D. degree from the University of Gdańsk (UG), Gdańsk, Poland, in 2007.

He was a Post-Doctoral Fellow with the Austrian Academy of Sciences, Vienna, Austria, and the Centre for Quantum Technologies (CQT), Singapore. He was an Assistant Professor with Nanyang Technological University, Singapore, and held a joint appointment at CQT. In 2019, he returned to UG as an Associate Professor. His works concern foundations of quantum physics, information theory, quantum computing, and (quantum) biology.

**Timothy C. H. Liew** received the Ph.D. degree in physics from the University of Southampton, Southampton, U.K., in 2008.

He was a Post-Doctoral Research Fellow with the National University of Singapore, Singapore, the École polytechnique fédérale de Lausanne, Lausanne, Switzerland, the Mediterranean Institute of Fundamental Physics, Rome, Italy, and Nanyang Technological University, Singapore, before being appointed as a Nanyang Assistant Professor at Nanyang Technological University in 2015. His interests include unconventional blockade mechanisms in quantum optics, topological effects in nonlinear systems (such as exciton–polaritons), optical neural networks, and quantum neural networks.